Electronic Supplementary Information (ESI†)

Hierarchical Porous Organic Polymers via In-Situ Construction of BINOL Entity: Versatile and Efficacious Adsorbents for Multiple Industrial Toxic Waste in Water

Flora Banerjee and Suman Kalyan Samanta*

Department of Chemistry, Indian Institute of Technology Kharagpur, Kharagpur 721302, India. E-mail: sksamanta@chem.iitkgp.ac.in

Table of Contents

1. Experimental Section

1.1. Materials and Methods. All the reagents, starting materials (α-naphthylamine, $FeCl_3$, 1,3,5-tribromobenzene, 4-bromoacetophenone), solvents and organic dyes were purchased from commercial suppliers and were used without further purification. Solvents were dried as per literature procedure prior to use according to the requirements. Thin layer chromatography (TLC) on silica gel GF_{254} was used for the determination of R_f values, and the visualization was performed by irradiation with UV lamp at 254 nm. Column chromatography was performed on Merck silica gel (100-200 mesh) with eluent as mentioned. ^1H (500 MHz) and ^{13}C (125 MHz) NMR spectra were recorded in a Bruker advance-500 NMR spectrometer in deuterated solvent at ambient temperature (300 K). Chemical shifts are reported in ppm (δ) relative to tetramethylsilane (TMS) as the internal standard ($CDCl_3$ δ 7.26 ppm for ^1H and 77.0 ppm for ^{13}C). Solid state ^{13}C CPMAS NMR spectra were recorded in a Bruker Ultrashield-500 NMR spectrometer. Mass spectra were recorded on Agilent 6500 Series Q-TOF spectrometer. Fourier transform infrared spectra (FTIR, 4000-600 cm^{-1}) were performed on Nicolet 6700 FT-IR spectrometer (Thermo Fischer) instrument, the wave numbers of recorded IR-signals are reported in cm^{-1}. Elemental analyses were carried out using a Perkin-Elmer Series-II, CHN/S Analyser-2400. Thermogravimetric analyses (TGA) were performed on a Pyris Diamond Tg Dta (PerkinElmer) instrument. The BINOL based porous organic polymers were observed under scanning electron microscope (SEM) model ZEISS SUPRA 40. The samples were prepared on aluminum stubs by adding powder polymers mounting on top of double-sided tapes. TEM measurements were carried out in a JEOL-2010EX machine operating at an accelerating voltage of 200 V. TEM samples were prepared by mounting on the copper grid for analysis. UV-visible adsorption spectra were recorded on a Shimadzu UV-2550 UV-vis spectrophotometer. X-Ray diffraction patterns of the powder organic polymer samples were obtained using a Bruker AXS D-8Advanced SWAX diffractometer using Cu-Kα (0.15406 nm) radiation. The N_2 adsorption/desorption isotherms of the sample was recorded on a Micromeritics 3-Flex Surface Characterization Analyzer at 77 K.

1.2. Chemical Synthesis

(a) Synthesis of 4-bromo-2-naphthol: Synthesis of the precursor 4-bromo-2-naphthol (**1**) was performed following a published procedure as reported by Newman *et al*. with minor modification.[1]

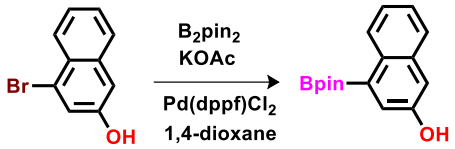

Scheme S1. Synthesis of precursor **2**

(b) Synthesis of 2: In a 2-neck round bottom flask, [Pd(dppf)]Cl_2.DCM (0.19 g, 0.27 mmol) was added to a degassed solution of 4-bromo-2-naphthol (**1**) (1.00 g, 5.32 mmol), bis(pinacolato)diboron (1.99 g, 7.98 mmol) and KOAc (0.88 g, 7.98 mmol) in dry1,4-dioxane. The reaction mass was heated to 100 °C for 12 h. Then the reaction mass was cooled to rt, filtered through Celite and concentrated in vacuo. Purification by silica gel column chromatography (10% ethyl acetate in hexane) afforded **2** (0.965 g). Yield 80%. ^{1}H NMR (CD_3OD, 500 MHz, ppm) δ 8.58 (1H, d); 7.59 (3H, m); 7.28-7.35 (2H, m); 1.34 (12H, s). ^{13}C NMR ($CDCl_3$, 125 MHz, ppm) δ 151.35, 133.83, 126.73, 112.17, 128.80, 123.07, 125. 84, 125.33, 108.48, 116.74, 82.58, 23.92. IR (KBr pellets, cm^{-1}): 3260, 1540,1260, 1140, 860, 765. HRMS: 269.0139 (calc.); 269.6138 (obs.)

(c) Synthesis of 1,3,5-tris(4-bromophenyl) benzene: Synthesis of the precursor 1,3,5-tris(4-bromophenyl) benzene was achieved using a literature reported procedure from commercially available 4-bromoacetophenone.[2]

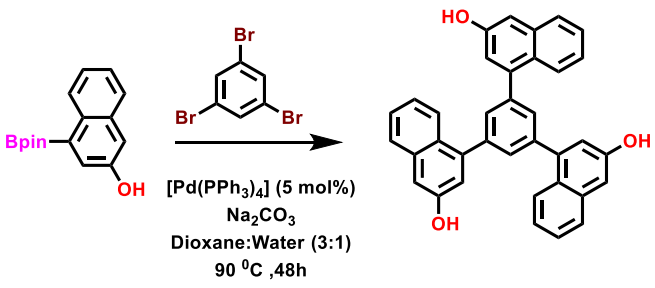

Scheme S2. Synthesis of monomer **3**

(d) Synthesis of monomer 3: 1,3,5-tribromobenzene (75 mg, 0.246 mmol) along with compound **2** (400 mg, 1.486 mmol), [Pd (PPh_3)$_4$] (5 mol% ,13.29 mg) in dioxane/H_2O (3:1)

was stirred at 90 °C under argon for 48 hours. Then the reaction mixture was allowed to cool to room temperature, quenched with water and extracted with ethyl acetate. The organic layer was washed with brine, dried over Na_2SO_4 and concentrated *in vacuo*. The residue was purified by flash column chromatography on silica gel (chloroform/methanol = 20:1) to afford the compound **3** as brown solid (80% yield). ^{1}H NMR ($CDCl_3$, 500 MHz, ppm) δ 8.05 (1H, d); 7.74 (1H, d); 7.72 (1H, s); 7.43 (1H, m); 7.32 (1H, m); 7.23 (1H, d); 7.18 (1H, d). ^{13}C NMR ($CDCl_3$, 125 MHz, ppm) δ 152.14, 140.81, 139.34, 134, 129, 126.26, 125.93,125.57, 124.93, 122.99, 118.09, 108.51. FT-IR (KBr pellets, cm^{-1}): 3405, 2975,1532,1276,1160, 860. HRMS: 504.1725 (calc.); 504.1790 (obtained). Elemental analysis C 85.69; H 4.79 (wt.%) (calc.); C 86.16; H 5.14 (wt.%) (obs.).

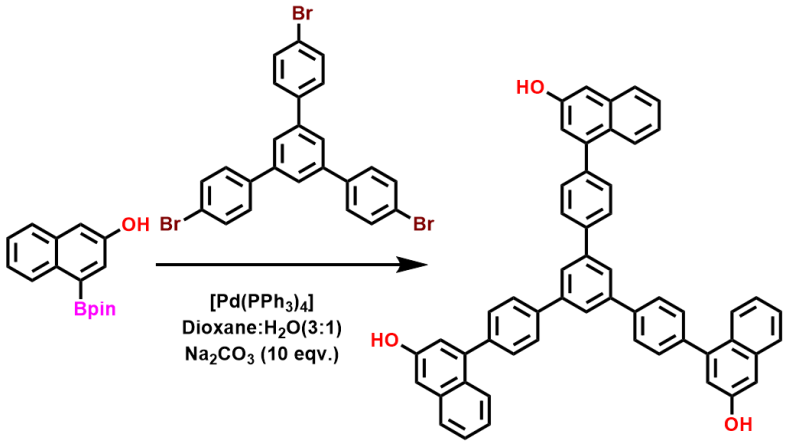

Scheme S3. Synthesis of precursor **4**

(e) Synthesis of monomer 4: Precursor **4** was synthesized under similar condition to precursor **3** taking 1,3,5-tris(4-bromophenyl) benzene instead of 1,3,5-tribromobenzene with an overall yield of 74%. In a 2-neck round bottom flask, 1,3,5-tris(4-bromophenyl)benzene (134 mg, 0.246 mmol) along with compound **2** (400 mg, 1.486 mmol), Na_2CO_3 (260 mg, 2.46 mmol) and [$Pd(PPh_3)_4$] (5 mol%, 34 mg) in dioxane/H_2O (3:1) was stirred at 90 °C under argon for 48 hours. Then reaction mixture was allowed to cool to room temperature, quenched with water and extracted with ethyl acetate. The organic layer was washed with brine, dried over Na_2SO_4 and concentrated *in vacuo*. The residue was purified by flash column chromatography on silica gel (chloroform/methanol = 25:1) to afford the compound **4** as orange solid (74% yield). ^{1}H NMR ($CDCl_3$, 500 MHz, ppm). δ 8.1 (1H, d); 7.92 (3H, m); 7.78(1H, d); 7.66(2H, d); 7.48(1H, m); 7.35(1H, m); 7.24(1H, d); 7.19(1H, d). ^{13}C NMR. ($CDCl_3$, 125 MHz, ppm) δ 153.69, 141.55, 139.66, 133.07, 132.12, 129.84, 129.76, 128.96, 128.89, 128.00, 124.89, 122.16, 118.83, 117.15, 109.57. FT-IR (KBr pellets, cm^{-1}): 3398, 2922, 1599, 1345,1170,778. HRMS:

732.2665 (calc.); 732.2732 (obtained). Elemental analysis: C 88.50; H 4.95 (wt%) (calc.); C 88.15; H 5.46 (wt%) (obs.)

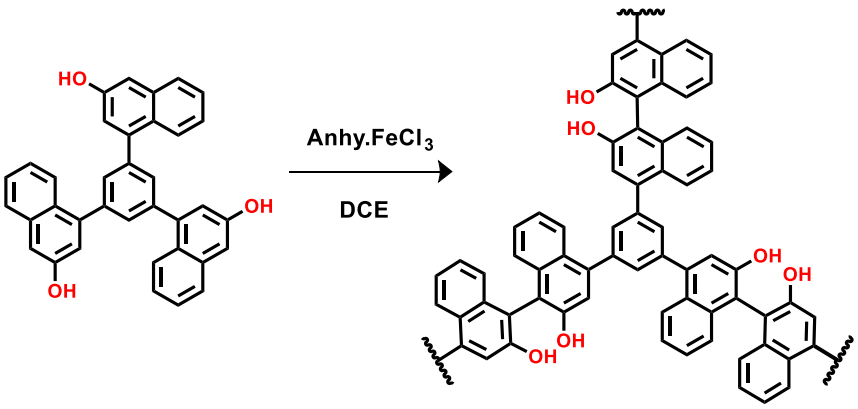

Scheme S4. Synthesis of polymer **BINOL-POP-1**

(f) Synthesis of polymer BINOL-POP-1: Precursor **3** (200 mg, 1 eqv.) was dissolved in anhydrous dichloroethane and anhydrous $FeCl_3$ (126 mg, 4.5 eqv.) was added to. The mixture was refluxed for 2 days. Then, the resulting precipitate was filtered and washed with dil. HCl and MeOH several times. The precipitate was again washed with $CHCl_3$, acetone and MeOH for 48 hours under Soxhlet extraction. Finally, it was dried under vacuum and the yellow polymer was obtained with 85% yield. IR (KBr pellets, cm^{-1}) 3458,2948,1576, 1180, 860. ^{13}C NMR (CP/MAS solid state, ppm) 152, 140, 127, 122, 118, 111. Elemental analysis C 85.20, H 5.72 (wt%) (calc.); C 85.52, H 5.23 (wt%) (obs.), TGA 5% wt. loss at 250°C.

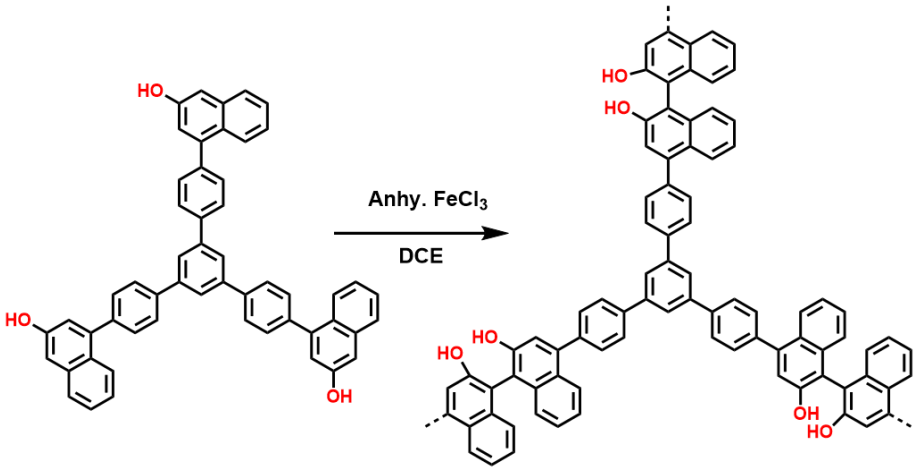

Scheme S5. Synthesis of **BINOL-POP-2**

(g) Synthesis of polymer BINOL-POP-2: BINOL-POP-2 was synthesized under similar condition taking precursor **4.** Precursor **4** (135 mg, 1 eqv.) was dissolved in anhydrous

dichloroethane and anhydrous $FeCl_3$ (130 mg, 4.5 eqv.) was added to it. The mixture was refluxed for 2 days. Then, the resulting precipitate was filtered and washed with dil. HCl and MeOH several times. The precipitate was again washed with $CHCl_3$, acetone and MeOH for 48 hours under Soxhlet extraction. Finally, it was dried under vacuum and brown polymer was obtained with 80% yield. IR 3468, 2926,1592, 1252,1174, 825. ^{13}C NMR (CP/MAS solid state, ppm) 153, 142, 141, 127,126, 118, 113, Elemental analysis C 86.98, H 5.03 (wt.%) (calc.); C 87.12, H 4.98 (wt.%) (obs.). TGA 5% wt. loss at 328°C.

1.3. Procedure for dye-adsorption:

In two separate vials, 1 mg of **BINOL-POP-1** and **BINOL-POP-2** each was added into a solution of a particular dye (20 μM) in ethanol. At first, the mixture was stirred for an hour at room temperature and then the vials were allowed to either stand for overnight for the precipitates to settle down or centrifuged at 4500 rpm to separate the adsorbed dye within the POPs from the suspension. Thereafter, the residual dye conc. in solution was determined from the UV-vis spectra. The spectra so obtained for each of the two solutions was compared to that of the parent dye in ethanol (20 μM) to obtain the removal efficiency for the BINOL-based POPs.

The removal efficiency for each dye was calculated using the following eqn.[3]

$$\textbf{Removal efficiency (RE) (in \%)} = [(C_0 - C_t)/ C_0] * 100$$

1.4. Monitoring kinetics of dye adsorption:

To get an insight into the kinetic details, 10 ml of 5 mg/L ethanolic solution of methylene blue dye was placed in the vial and 1 mg/ml of POP was added to it and mixed thoroughly using micropipette. The UV-Vis absorbance was checked after taking an aliquot from resulting suspension after stirring within certain time interval. The plot of abs. vs time was obtained after checking the absorbance of supernatant at each time interval probing the UV-Vis spectrophotometer at 664 nm wavelength. Similar method was repeated for all other dyes.

Thereafter, the plot was fitted with pseudo first order rate equation to get the rate constant value.

$$\ln(A/A_0) = e^{\wedge} (-kt)$$

1.5. Monitoring kinetics from aqueous solution:

For this purpose, 1 mg/ml of aqueous dispersion of BINOL-POP-1 was mixed with 10 ml aqueous solution of two of the as-taken analytes *i.e.* propidium iodide (66.8 mg/L) and ethidium bromide (39.4 mg/L) and thereafter stirred at room temperature. The UV-Vis absorbance data was collected after picking up 1 ml of aliquot from the resulting mixture at an interval of 10 seconds. Thus, obtained plot of absorbance vs. time was fitted very well with pseudo first order rate equation to obtain the rate constant value.

1.6. Adsorption isotherm:

To monitor the adsorption isotherm, eight different sets of aqueous solution with varying conc. in between 100-800 mg/L was prepared followed by adding 1 mg of **BINOL-POP-1** or **BINOL-POP-2** separately to it. The resulting suspension was stirred for an hour and settled down for overnight and then the supernatant was subjected to UV-Vis study. The equilibrium dye conc. $\mathbf{C_e}$ (mg/L) was obtained from absorbance data itself.[3]

The equilibrium adsorption capacity $\mathbf{Q_e}$ (mg/g) was obtained using the eqn. below

$$\mathbf{Q_e = [(C_0 - C_e)] * V / m}$$

Where, m = mass of adsorbent added, V = total volume of solution.

The isotherm was analyzed using both Langmuir equation.

$$\mathbf{C_e/Q_e = 1/(K_L Q_m) + C_e/Q_m}$$

And Freundlich equation as follows

$$\mathbf{\ln Q_e = \ln C_e + (1/n) \ln K_F}$$

The maximum adsorption capacity was measured from the slope of C_e/Q_e vs C_e plot from Langmuir equation.

1.7. Procedure for estimating the quantitative dye adsorption capacity manually:

In separate vials, 1 mg each of the **BINOL-POP-1** and **BINOL-POP-2** were weighed and added. A 374 mg/L methylene blue stock solution in milli pure water was prepared in another vial. From there, 20 μL of the methylene blue solution was taken accurately using a

micropipette and added to each vial containing the **BINOL-POP-1** and **BINOL-POP-2**.[4] Both the mixtures were stirred at room temperature until the dye was completely adsorbed by the POPs. Following that, another 20 μL of the methylene blue dye solution was added to each vial again and the stirring was continued until the dye was completely adsorbed as discerned from naked eye. This process was repeated for several times until the extent of dye adsorption finally reached an equilibrium in both the cases and the residual dye remained in the solution as confirmed from its blue color. The dye concentration was determined using UV-Vis spectra. Similar procedure was carried out for crystal violet, propidium iodide, ethidium bromide and neutral red.

1.8. Selectivity test:

To evaluate the selective dye adsorption capacity of **BINOL-POP-1** and **BINOL-POP-2**; each of 5 mg/L methylene blue and methyl orange were taken in ethanol and mixed together. After adding 1 mg of either of the POPs; the solution was stirred for 1h and allowed to settle down for overnight. The residual dye conc. was monitored using UV-Vis spectrophotometer. Both the BINOL-based POPs captured MB selectively with more than 99.9% efficiency. It was observed that residual solution contained the characteristic peak of MO at 440 nm.

1.9. Thermodynamics of Dye Adsorption:

For thermodynamic study of adsorption, 1 mg of BINOL-POP-1 was weighed in two separate vials and 1 ml of water was added to it. On the other hand, a 668 mg/L stock solution of Propidium iodide (1 mM) and 394 mg/L (1 mM) solution of Ethidium bromide was prepared in water. 20 μL from the parent stock solution was added each time to the vials until the dye gets adsorbed over the POP as discerned from naked eye. This process was repeated several times until the adsorbent reaches its saturation as confirmed from the UV-Vis spectra. Thus, obtained equilibrium adsorption capacity (Q_e) and equilibrium concentration (C_e) were utilized in the following equation to get the free energy change (ΔG) value at three different temperatures 300 K, 310 K, 320 K.[5]

The distribution co-efficient is represented as, $\mathbf{K_d = Q_e/C_e}$

$$\text{Now} \quad \mathbf{\Delta G = -RT \ln K_d}$$

Using Vant-Hoff equation, ΔH; ΔS for the adsorption process can be determined.

$$\mathbf{\ln K_d = - \Delta H/(RT) + \Delta S/R}$$

From the above equation, the plot of $\ln K_d$ vs 1/T gives a straight line with a slope = - $\Delta H/R$ and an intercept of $\Delta S/R$. Thus, we can get the values of Gibbs free energy change, enthalpy and entropy changes for adsorption at a particular temperature for dye adsorption.

1.10. Recyclability test:

To evaluate the recyclability of our as synthesized POPs, first the dye loaded POP was filtered and washed rigorously with MeOH containing 0.1M HCl until the filtrate becomes colorless as discerned from naked eye. Thereafter, the adsorbent was dried under vacuum and put through the next cycle.

2. Characterizations

a)

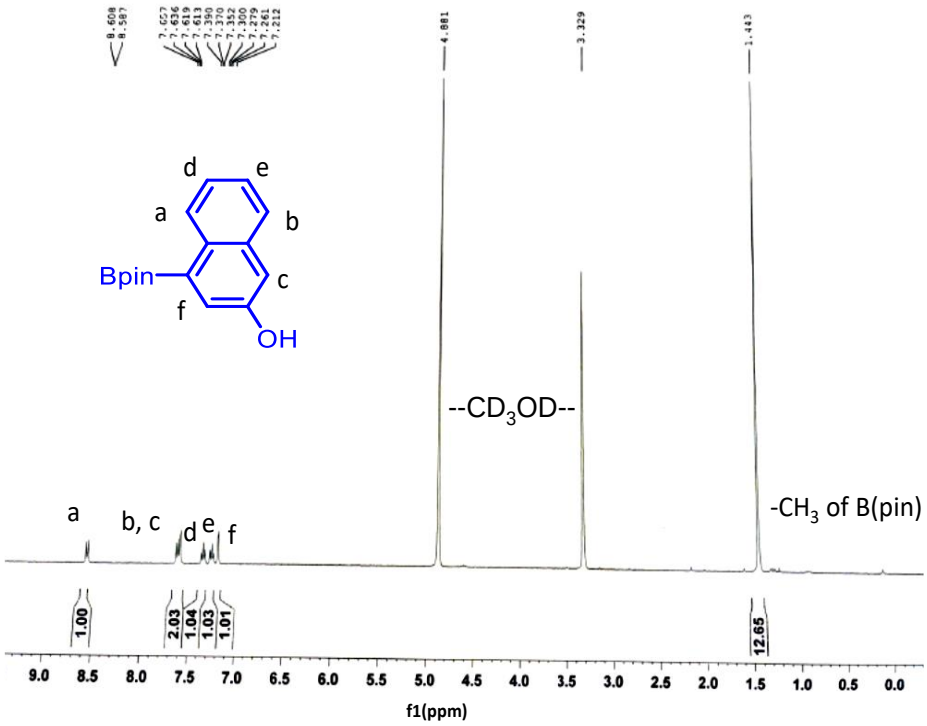

b)

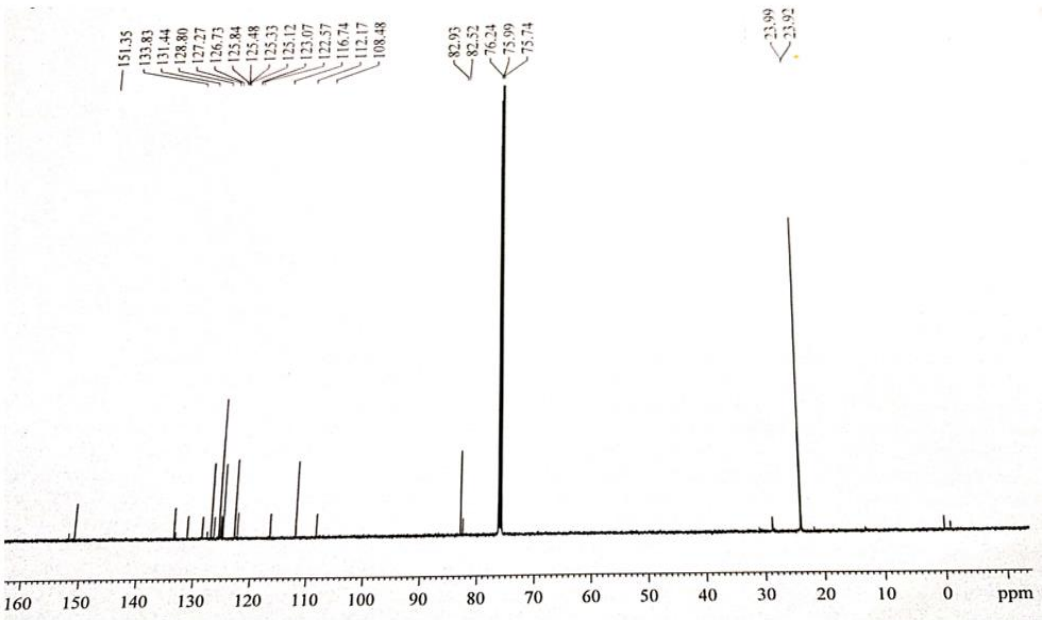

Fig.. S1 a) ^{1}H NMR (CD_3OD) and b) ^{13}C NMR ($CDCl_3$) of precursor **2**.

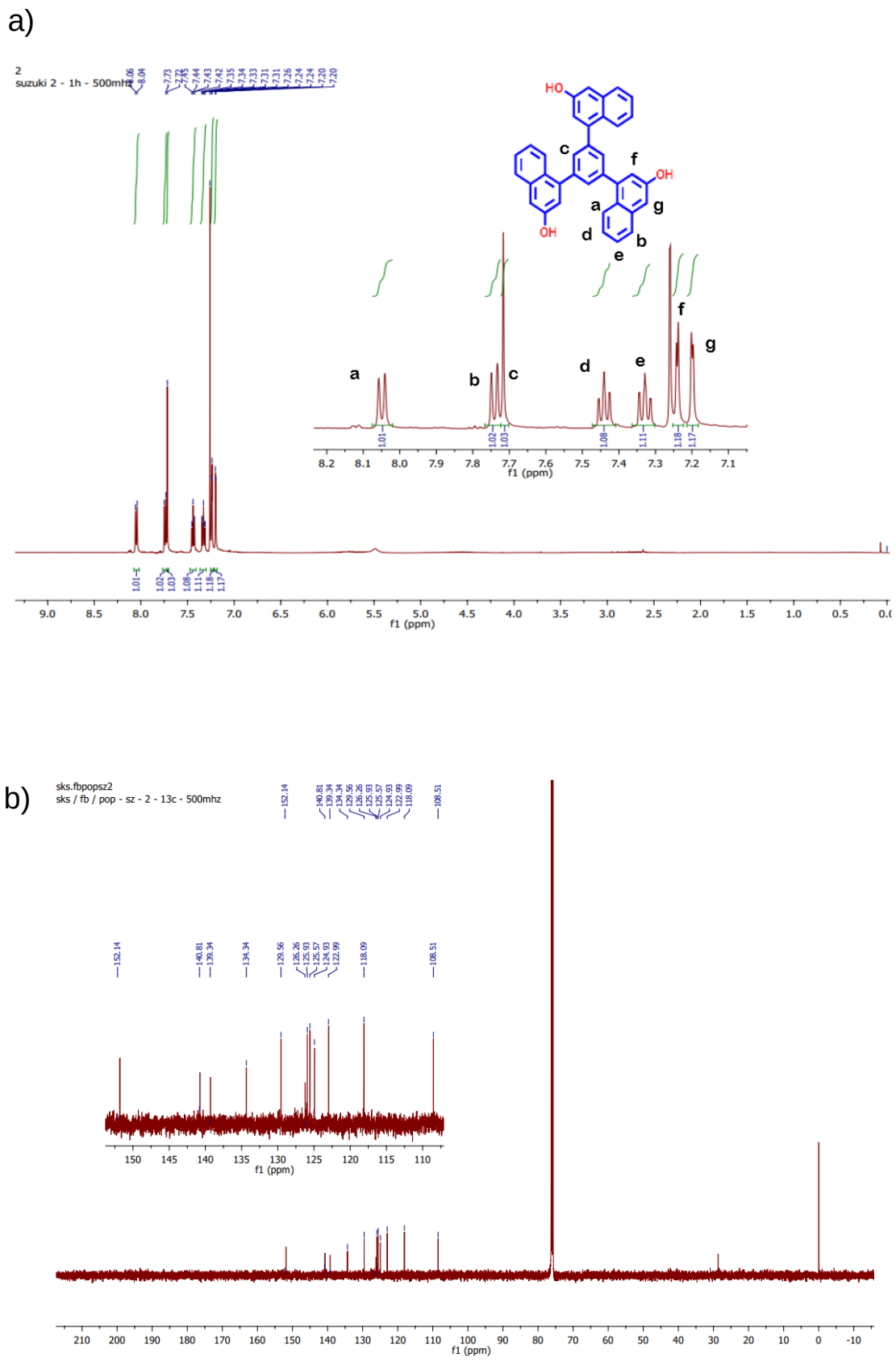

Fig. S2 (a) ^{1}H NMR and (b) ^{13}C NMR of precursor **3** in $CDCl_3$.

a)

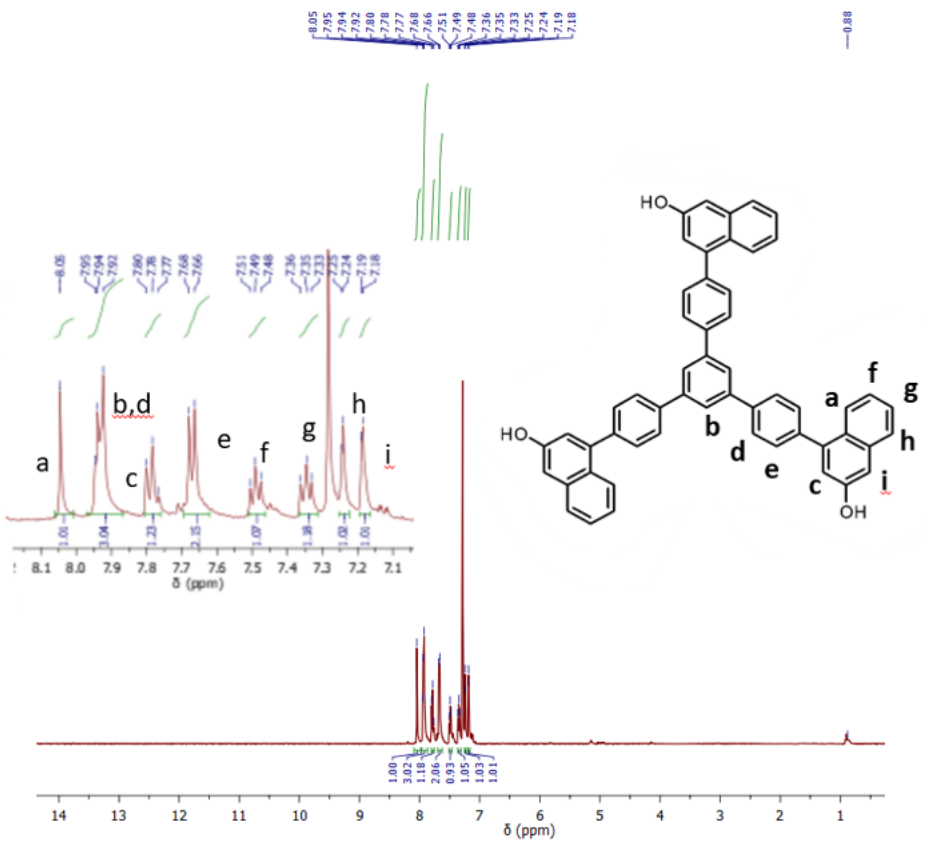

b)

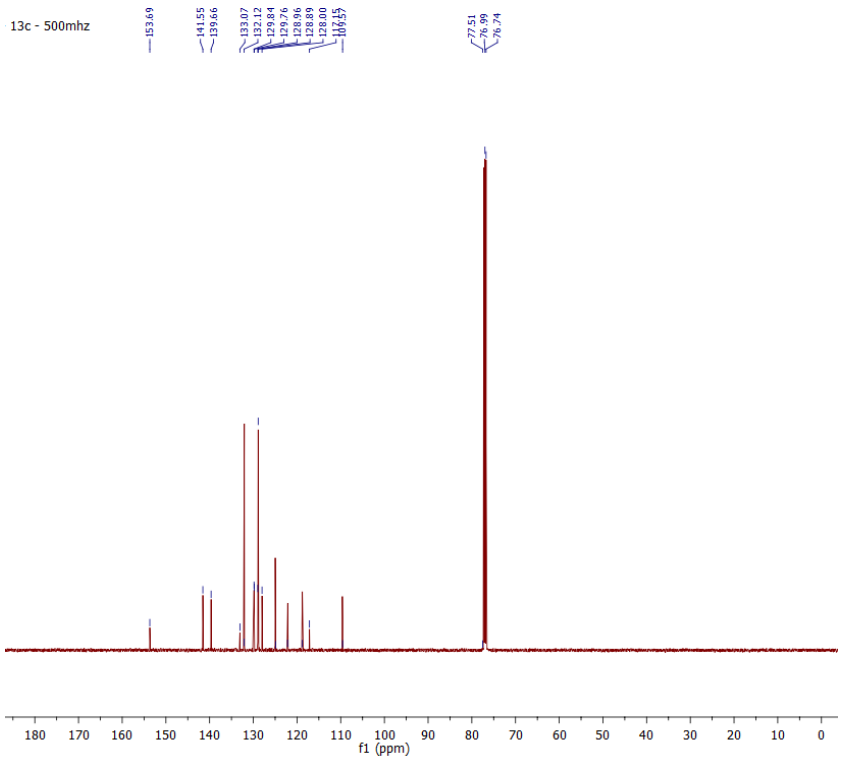

Fig. S3 a) ^{1}H and b) ^{13}C NMR of precursor **4** in $CDCl_3$.

2.4. FT-IR spectra of precursor 4 and BINOL-POP-2

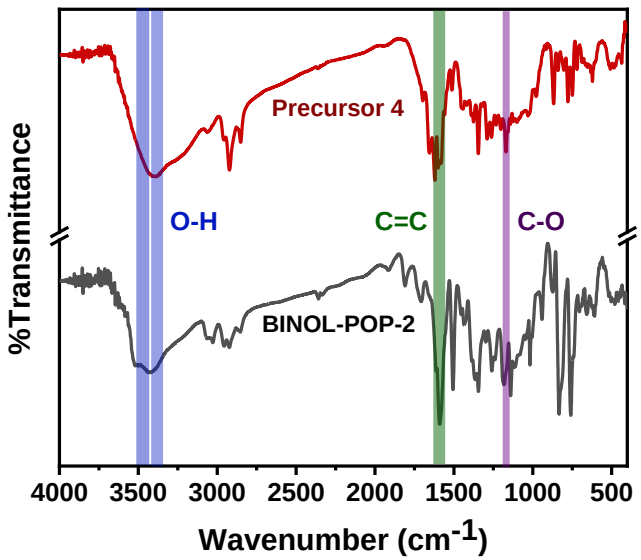

Fig. S4 FT-IR spectra of the **BINOL-POP-2** in comparison to the corresponding monomer **4** (in KBr pellets).

2.5. ^{13}C CP/MAS solid state NMR

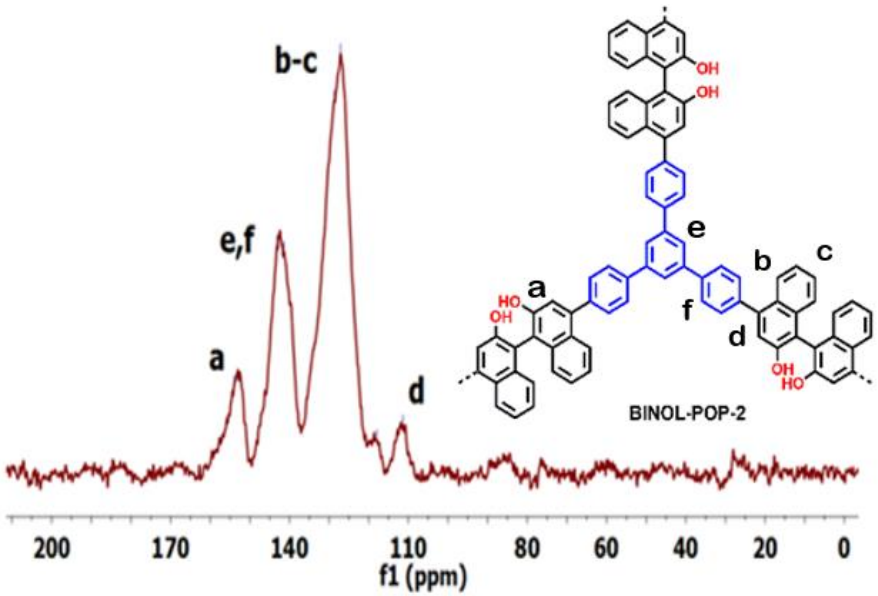

Fig. S5 Solid state ^{13}C CP/MAS NMR of **BINOL-POP-2.**

2.6. Morphological Studies

a)

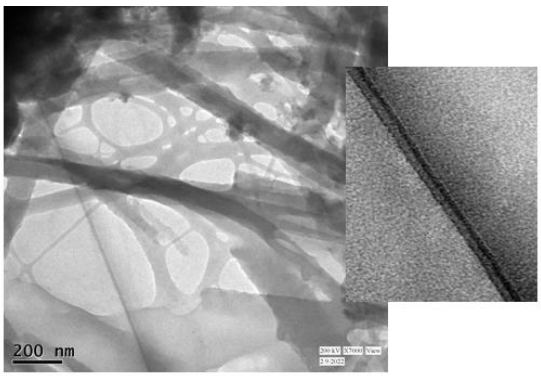

b)

Element	Wt %	At %
C K	86.29	89.35
O K	13.70	10.65
ClK	00.01	00.00
FeK	00.00	00.00

c)

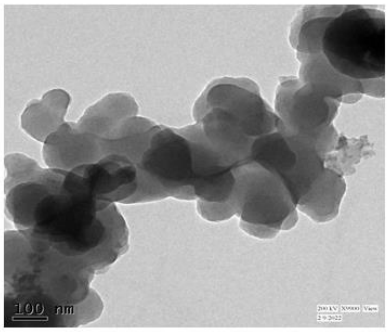

d)

Element	Wt %	At %
C K	92.41	94.21
O K	07.55	05.78
ClK	00.01	00.00
FeK	00.00	00.00

Fig. S6 a) TEM image of **BINOL-POP-1** (inset – zoomed in view of a single hollow tube) and b) the corresponding EDAX profile. c) TEM image for **BINOL-POP-2** and e) the EDAX pattern. The EDAX pattern showed higher oxygen content for **BINOL-POP-1** compared to **BINOL-POP-2**, in accordance with their chemical structure.

3. Dye Adsorption Studies

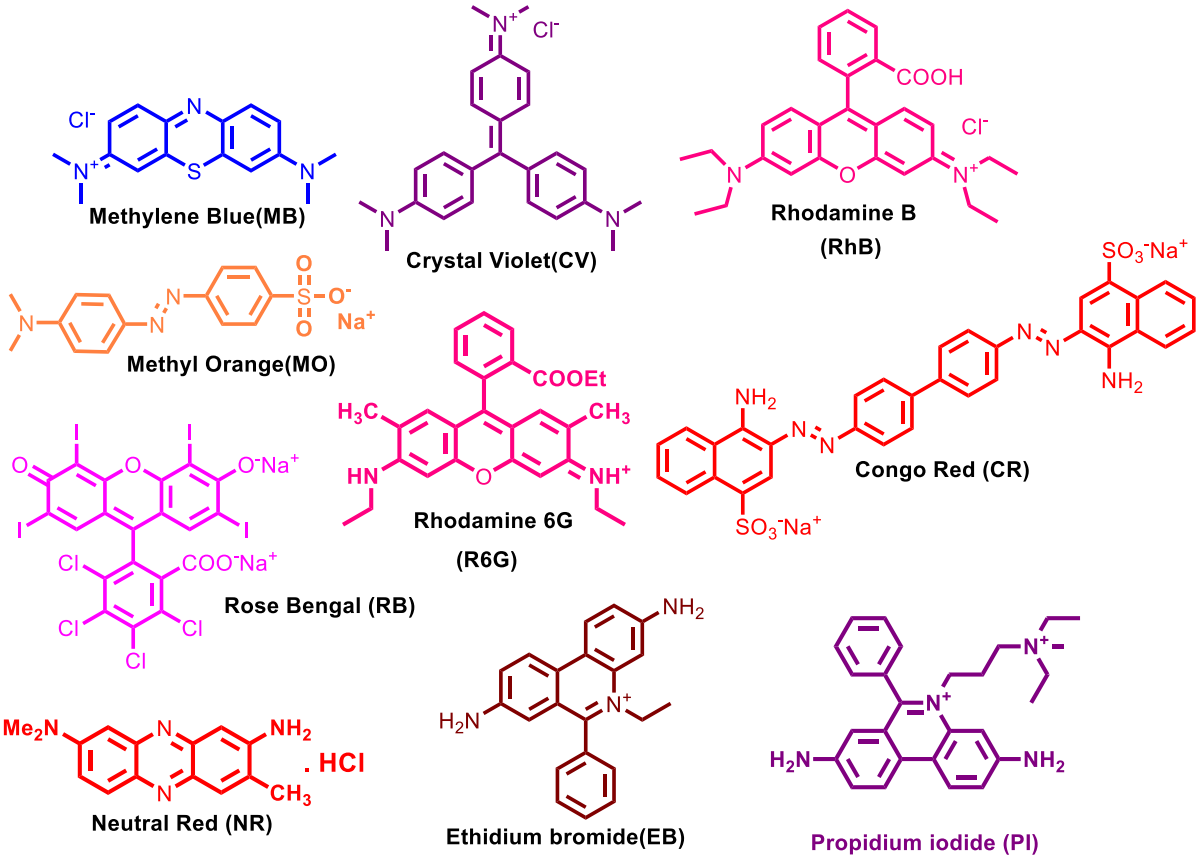

Fig. S7 Cationic and anionic dyes for the adsorption by **BINOL-POP-1** and **BINOL-POP-2**.

3.1 Removal efficiency (RE) from UV-Vis spectra

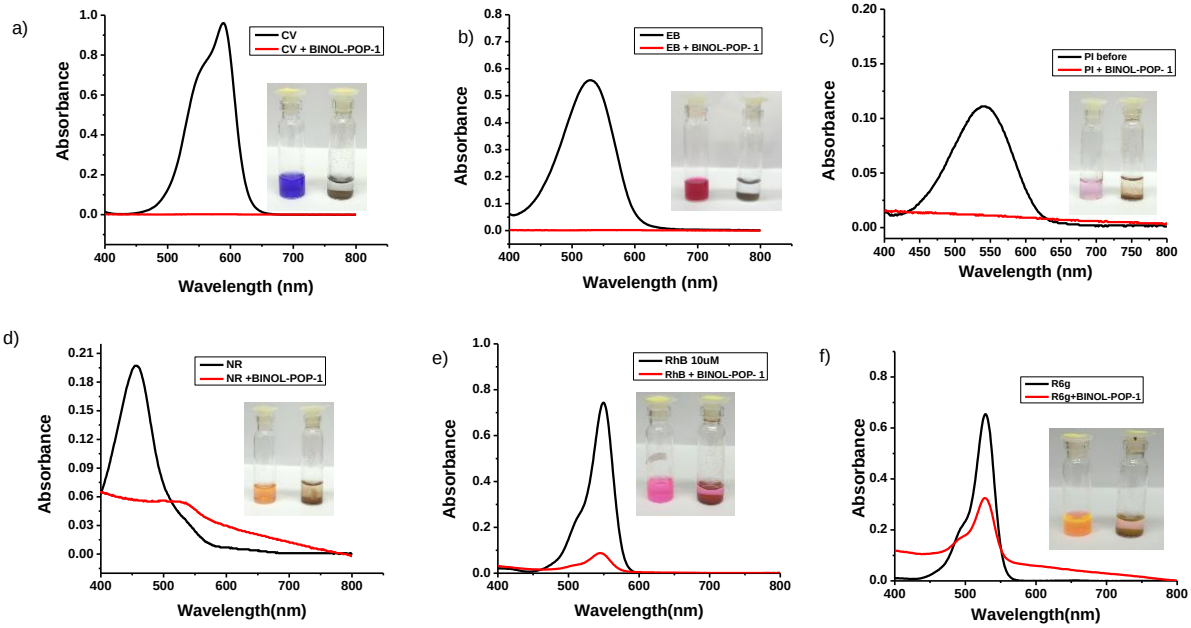

Fig. S8 UV-Vis spectra for the removal of cationic dyes a) crystal violet (CV), b) ethidium bromide (EB), c) propidium iodide (PI), d) neutral red (NR), e) rhodamine B (RhB), and f) rhodamine 6G (R6G) using **BINOL-POP-1**. Dye concentration was 0-50 mg/L in ethanol and 1 mg of the POP was added to it.

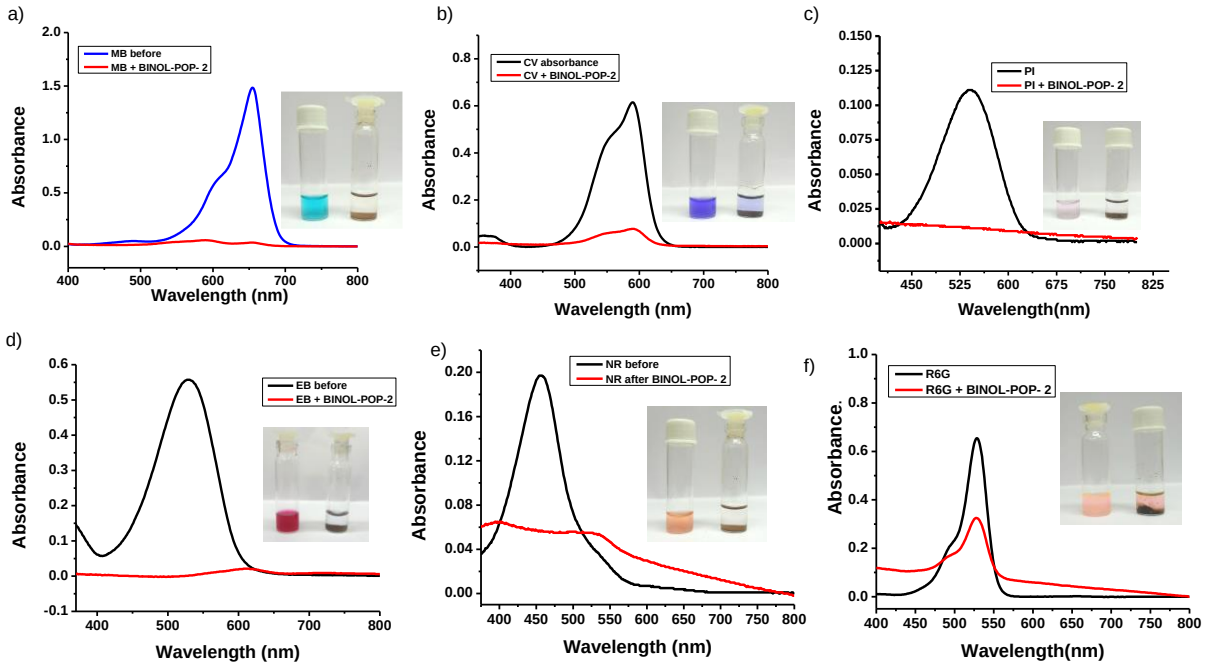

Fig. S9 UV-Vis spectra for the removl of cationic dyes a) methylene blue (MB), b) crystal violet (CV), c) propidium iodide (PI), d) ethidium bromide (EB), e) neutral red (NR) and f) rhodamine 6G (R6G) by **BINOL-POP-2**. Dye concentration was 0-50 mg/L in ethanol and 1 mg of the POP was added to it.

Table S1. Comparative study of removal efficiency for **BINOL-POP-1** and **BINOL-POP-2** towards various dyes.

Adsorbent	Methylene blue	Crystal violet	Ethidium bromide	Propidium iodide	Neutral Red	Rhodamine 6G	Rhodamine B
BINOL-POP-1	100	100	100	100	84	52	75
BINOL-POP-2	100	95	100	100	82	49	70

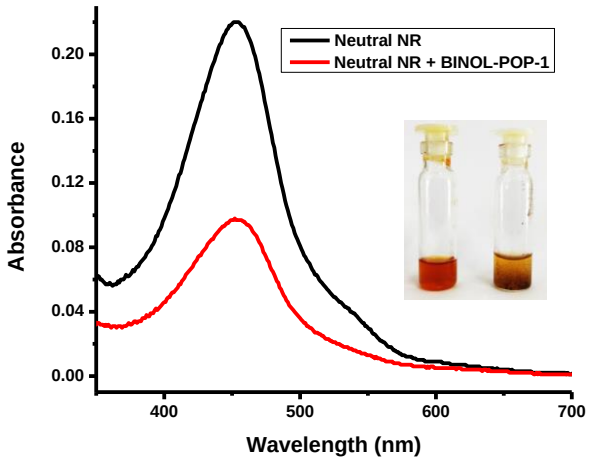

Fig. S10 Adsorption of neutral red (in neutral state) monitored by UV-Vis spectra (measured at λ_{max} 453 nm). Inset showing the corresponding vials for the adsorption of neutral red dye.

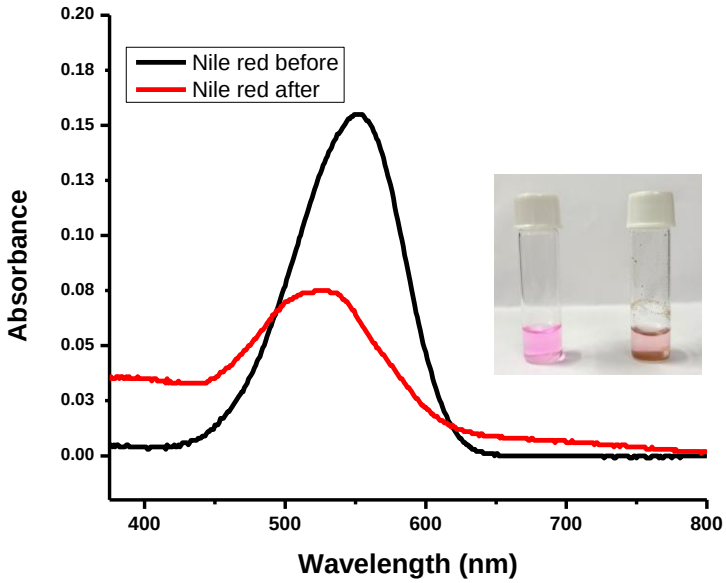

Fig. S11 Absorbance of Nile red before (black) and after adding **BINOL-POP-1** (red). Inset showing the corresponding vials for the adsorption of Nile red dye. UV-Vis spectra unveiled partial adsorption for Nile red with a slight blue shift in absorption maxima at 562 nm.

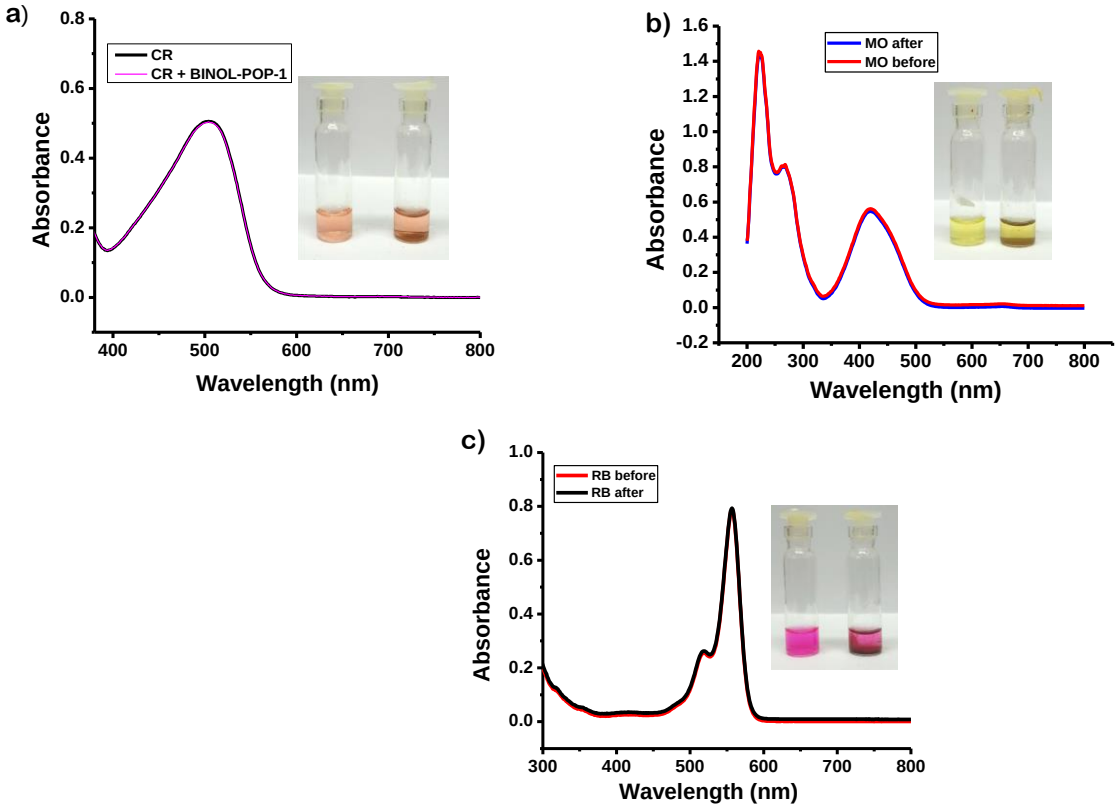

Fig. S12 UV-Vis spectra for a) Congo red (CR); b) methyl orange (MO); and c) rose bengal (RB) before and after adding **BINOL-POP-1**. In case of anionic dyes, the dye uptake was monitored under similar condition.

3.2 SELECTIVITY TEST

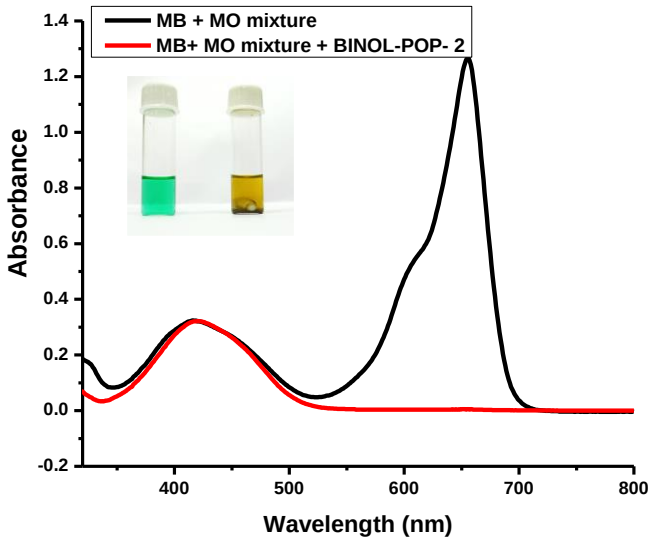

Fig. S13 UV-Vis spectra for selectivity test for **BINOL-POP-2**.

3.3 Kinetic adsorption experiment

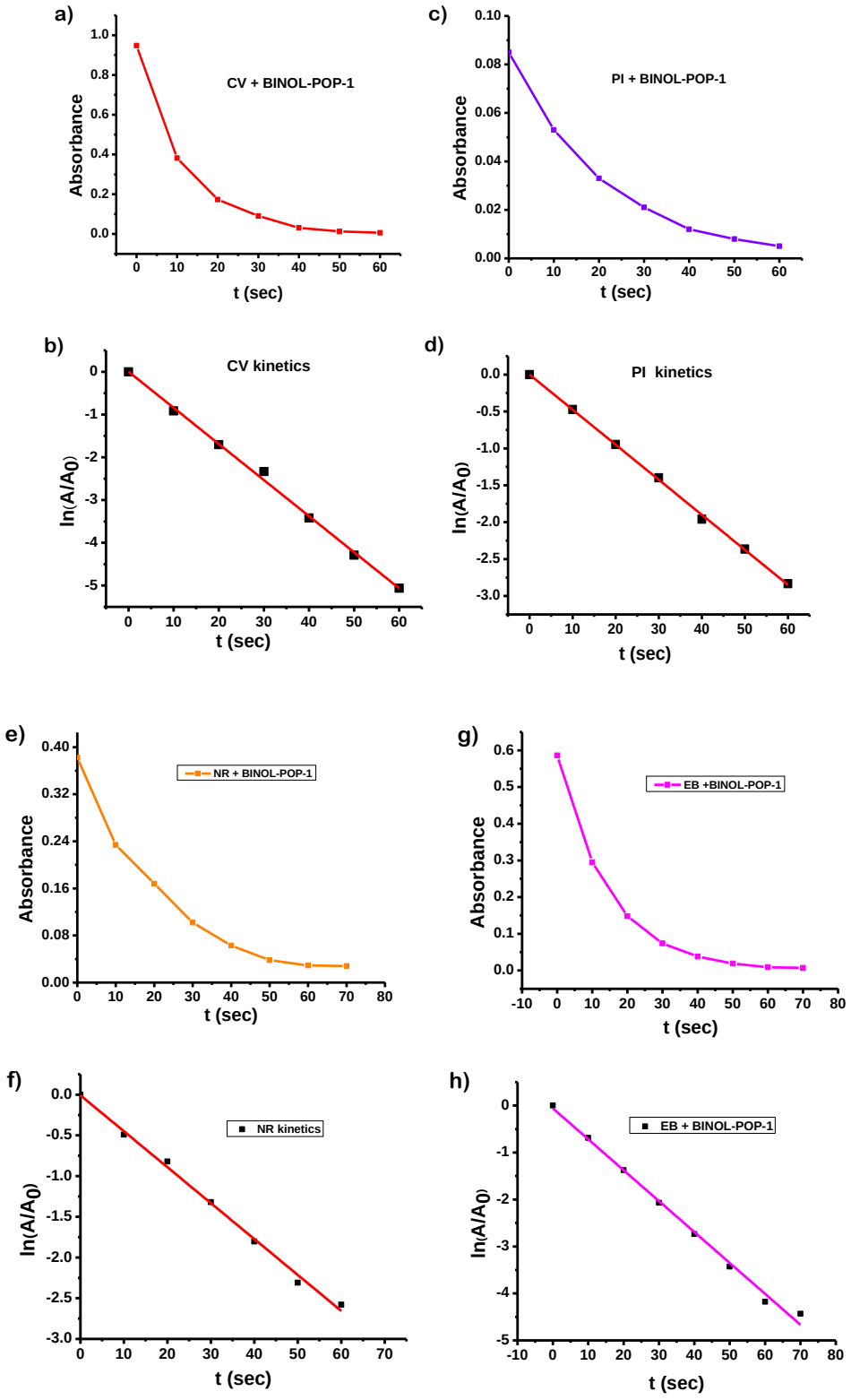

Fig. S14 Kinetic studies for CV, PI, NR and EB respectively in presence of **BINOL-POP-1** (1 mg/ml) showing that the pseudo first order rate equation fits well with the data obtained for each dye.

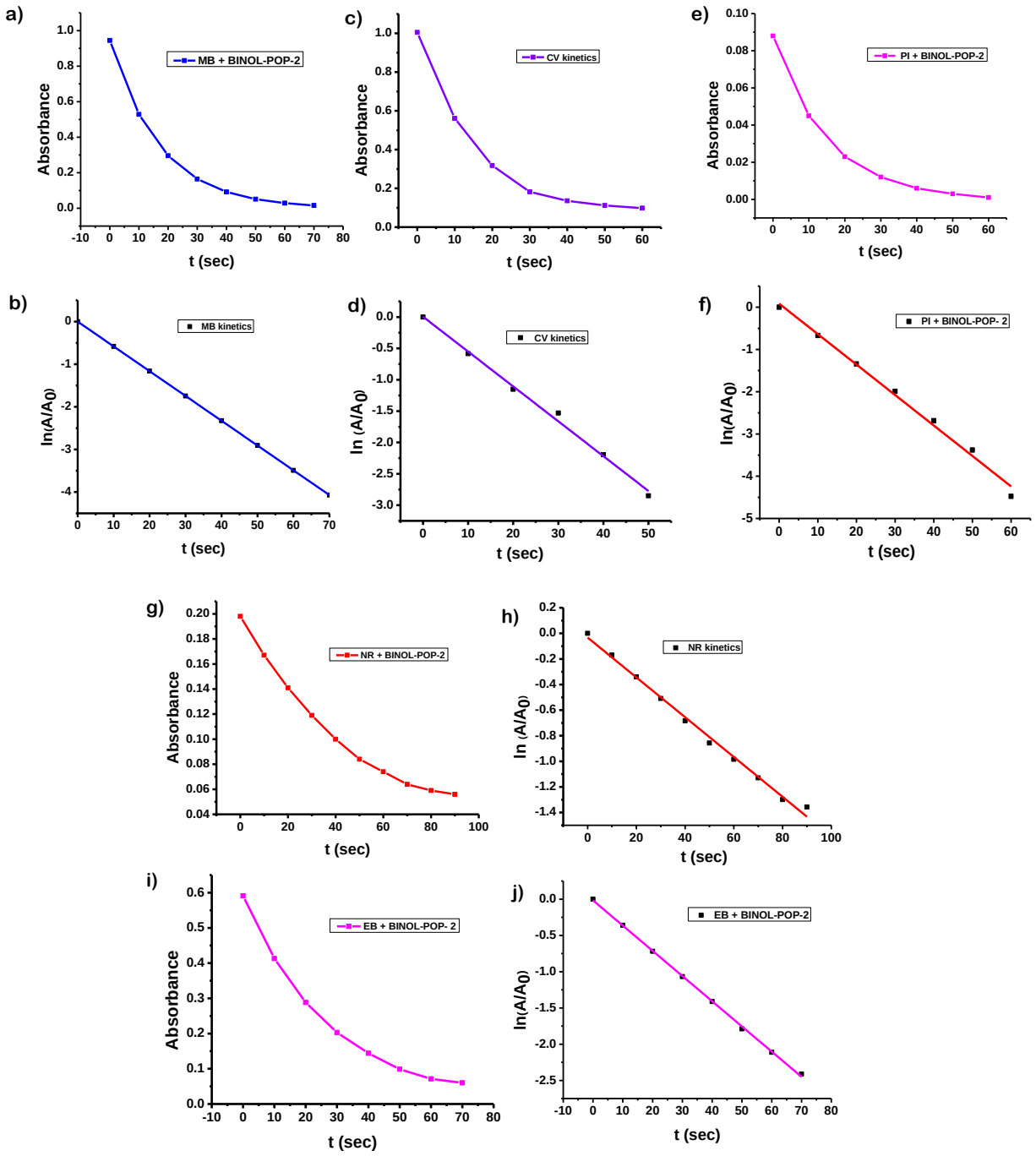

Fig. S15 Kinetic studies for MB, CV, PI, NR and EB respectively in presence of **BINOL-POP-2** (1 mg/ml) showing pseudo first order rate equation fits well with data obtained for each dye.

Table S2. Comparison of kinetic data (k, min^{-1}) for **BINOL-POP-1** and **BINOL-POP-2**.

Material	Methylene Blue	Crystal Violet	Propidium Iodide	Ethidium Bromide	Neutral Red
BINOL-POP-1	5.21	5.09	4.33	3.95	2.65
BINOL-POP-2	3.49	3.31	2.71	2.09	0.94

Kinetic studies for dye adsorption from water:

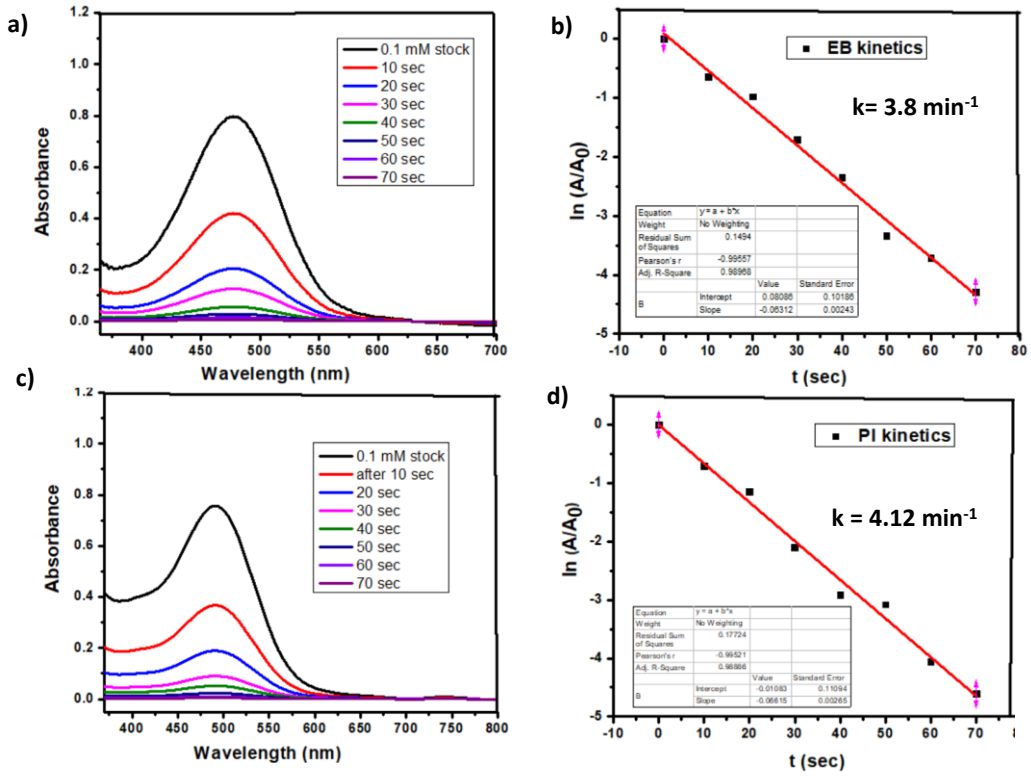

Fig S16. The absorbance vs. time plot and pseudo first order fitting results for ethidium bromide (a,b) and propidium iodide (c,d) with **BINOL-POP-1** (1 mg/ml).

3.4. Calculation of Maximum Adsorption Capacity

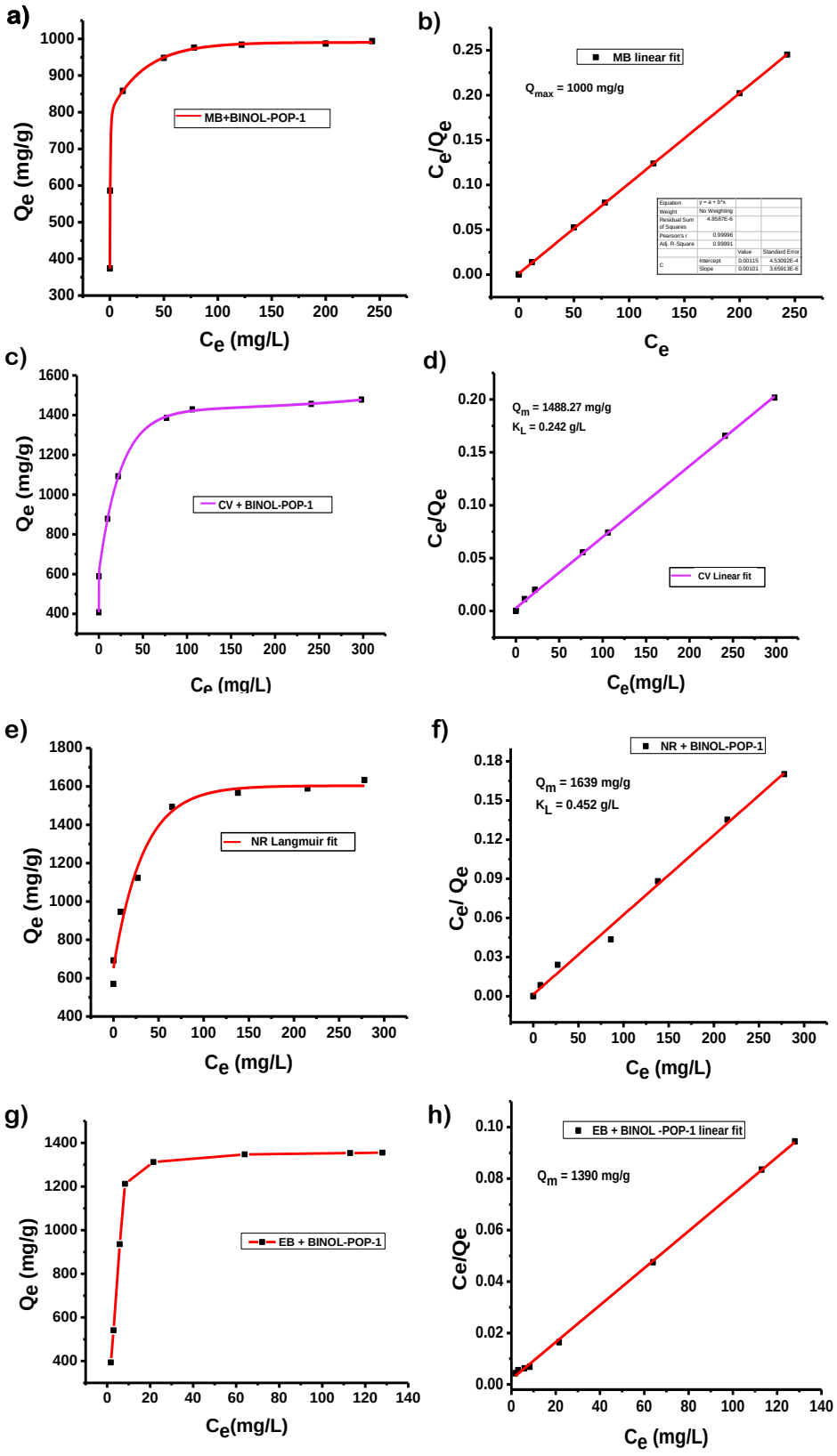

Fig. S17 Adsorption isotherm and Langmuir fitting for cationic dyes MB (a, b); CV (c, d); NR (e, f) and EB (g, h) for **BINOL-POP-1** respectively.

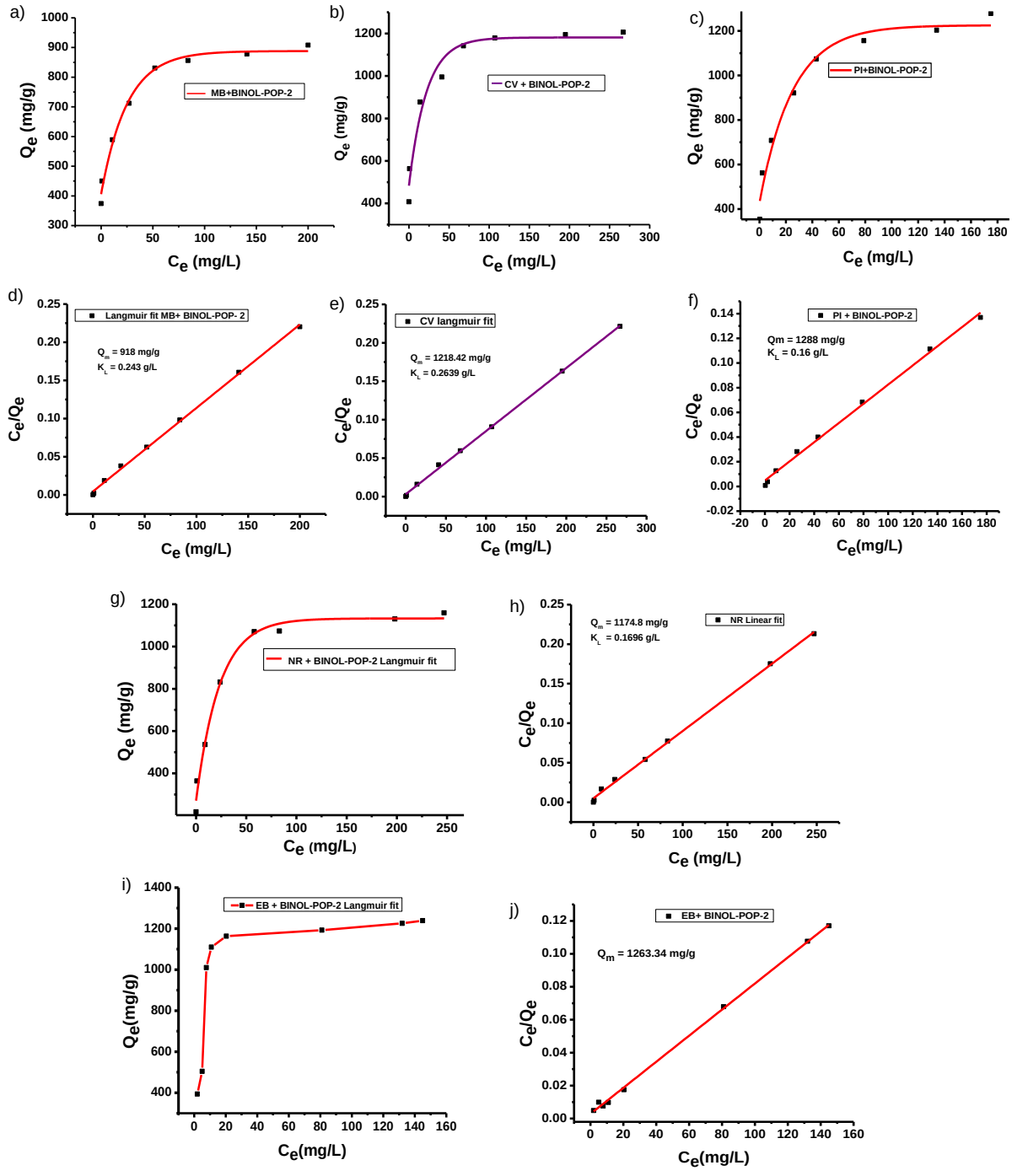

Fig. S18 Adsorption isotherm and Langmuir fitting model for **BINOL-POP-2** with methylene blue (a, b); crystal violet (c, d); propidium iodide (e, f); neutral red (g, h); ethidium bromide (i, j).

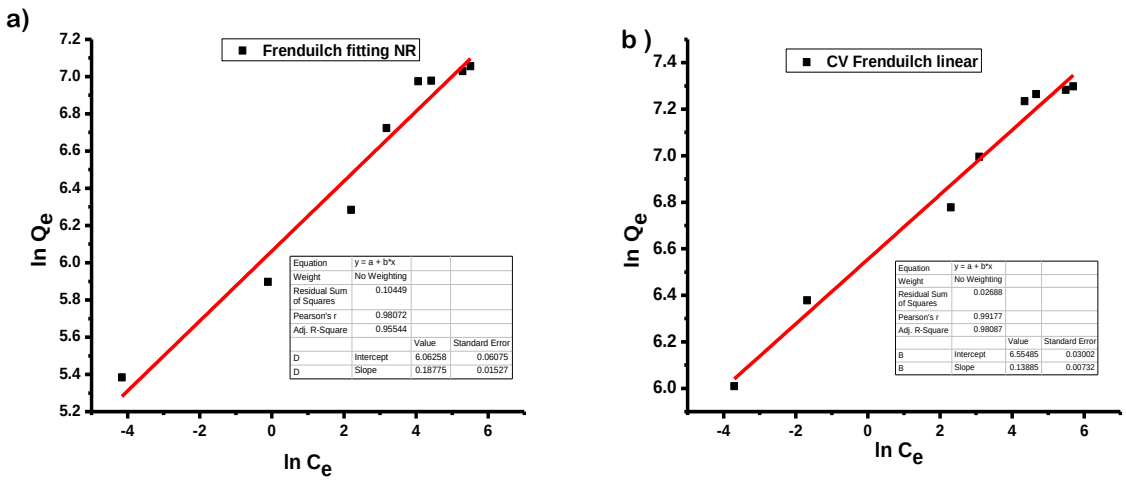

Fig. S19 Freundlich fitting for **BINOL-POP-2** with a) neutral red and b) crystal violet showing $R^2 < 0.99$ value.

Table S3. Summary of the Freundlich isotherm model fitting results (R^2 value).

	Methylene Blue	**Crystal Violet**	**Propidium Iodide**	**Ethidium Bromide**	**Neutral Red**
BINOL-POP-1	0.9842	0.9674	0.9781	0.9765	0.9822
BINOL-POP-2	0.9812	0.9808	0.9654	0.9824	0.9554

Table S4. Comparative Q_{max} values obtained manually and from the Langmuir model for **BINOL-POP-1**.

Dyes	**Q_{max} obtained from Langmuir model**	**Q_{max} obtained manually**
Methylene Blue	1000	973
Crystal Violet	1488	1457
Ethidium Bromide	1390	1377
Propidium Iodide	1941	1905
Neutral Red	1639	1589

3.5 Comparison of Adsorbents for the Tested Dyes

Table S5. Comparison of adsorbents for crystal violet.

Adsorbent	Q_{max} data (mg/g)	Reference
HPP-3	862	Ge *et al.*[6]
FC-HPP	1085	Yang *et al.*[7]
DPPF-HPP	1440	Yang *et al.*[8]
MDBC 800	1223	Chen *et al.*[9]
CTT-POP-1	1685	Zhang *et al.*[3]
CTT-POP-2	1374	Zhang *et al.*[3]
HAzo-POP-1	1204	Zhang *et al.*[3]
BINOL-POP-1	**1488**	**This work**
BINOL-POP-2	**1218**	**This work**

Table S6. Comparison of adsorbents for methylene blue.

Adsorbent	Q_{max} (mg/g)	Reference
BOPs	3250	Zhao *et al.*[10]
CMP-YA	1016	Yuan *et al.*[11]
MOP-2	1153	Huang *et al.*[12]
LCHPP-2	667	Du *et al.*[13]
POMs	400	Valley *et al.*[14]
POP-TFP-COOH	2740	Yan *et al.*[15]
CTT-POP-1	1239	Zhang *et al.*[3]
CTT-POP-2	926	Zhang *et al.*[3]
BINOL-POP-1	**1000**	**This work**
BINOL-POP-2	**918**	**This work**

Table S7. Comparison of adsorbents for propidium iodide.

Adsorbent	Q_{max}	Reference
ND-MOz	200	Gibson *et al.*[16]
RUDDM 1	85	Gibson *et al.*[17]
BINOL-POP-1	**1941**	**This work**
BINOL-POP-2	**1288**	**This work**

Table S8. Comparison of adsorbents for neutral red.

Adsorbent	Q_{max}	Reference
Fe_3O_4 hollow spheres	105	Iram *et al.*[18]
SB-β-CD	685	Mpatani *et al.*[19]
BINOL-POP-1	**1639**	**This work**
BINOL-POP-2	**1174**	**This work**

Table S9. Comparison of adsorbents for ethidium bromide.

Adsorbent	Q_{max}	Reference
NP	58.82	Heibati *et al.*[20]
ACP	76.92	Heibati *et al.*[20]
NIFSS	131.78	Sulthana *et al.*[21]
BINOL-POP-1	**1390**	**This work**
BINOL-POP-2	**1263**	**This work**

3.6 COMPUTATIONAL DETAILS

The ground states of the molecules were optimized using the DFT/B3LYP method [22,23] with the 6-31++G* basis set in Gaussian16.[24] To generate the ESP maps, Gaussview[25] was used. The complex structures of the repeating unit of host POP with crystal violet and methylene blue were optimized using the dispersion corrected DFT method with BJ damping.[26,27] The complexation energies were calculated using the supermolecular approach.[28,29] Counterpoise method was used to remove the basis set superimposition error (BSSE).[30]

a)

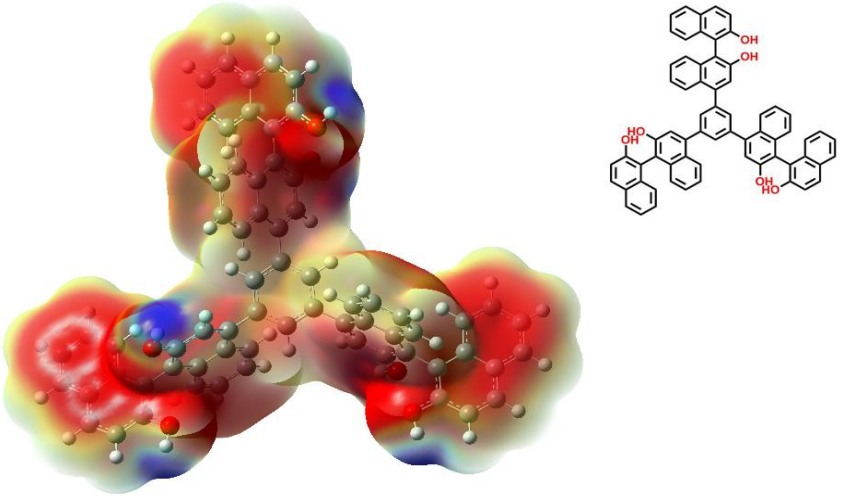

ESP map of model host unit. Surface potential ranges from −0.015000 au (red) to 0.050000 au (blue). Isovalue is 0.000400 au.

b)

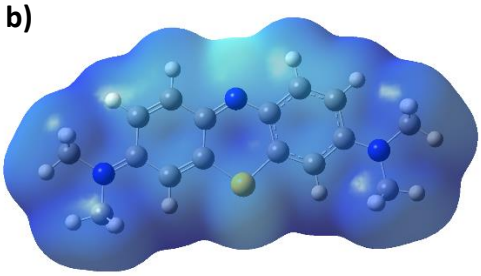

c)

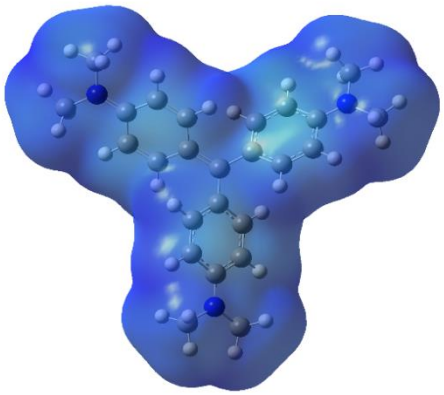

ESP map of methylene blue and crystal violet. Surface potential ranges from −0.122000 au (red) to 0.122000 au (blue). Isovalue is 0.000400 au.

Fig. S20 ESP mapping diagram for the a) model host unit, b) methylene blue and c) crystal violet dye.

3.7 Zeta potential analysis

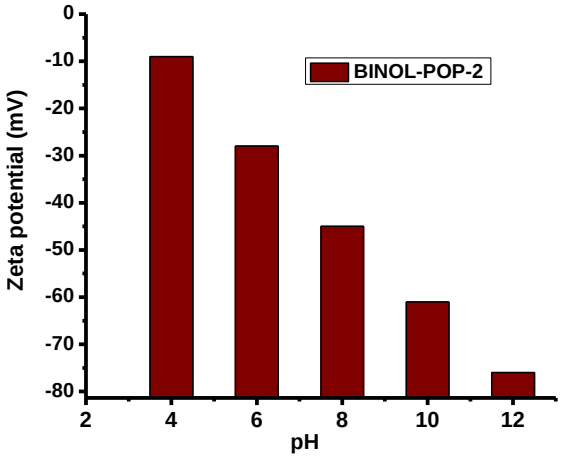

Fig. S21 Zeta potential study for **BINOL-POP-2** under different pH.

Table S10. Comparison of surface charge (in mV) at different pH between **BINOL-POP-1** and **BINOL-POP-2.**

Polymer	at pH 4	at pH 6	at pH 8	at pH 10	at pH 12
BINOL-POP-1	**-23**	**-42**	**-75**	**-92**	**-107**
BINOL-POP-2	**-9**	**-28**	**-45**	**-61**	**-76**

3.8. Counter ion effect:

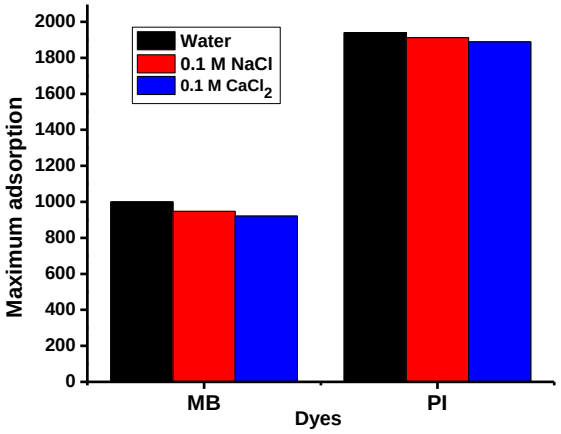

Fig. S22 The maximum dye adsorption capacity of **BINOL-POP-1** in water (black); or in presence of 0.1 M NaCl (red); and 0.1 M $CaCl_2$ (blue) for MB and PI.

3.9 Adsorption thermodynamics:

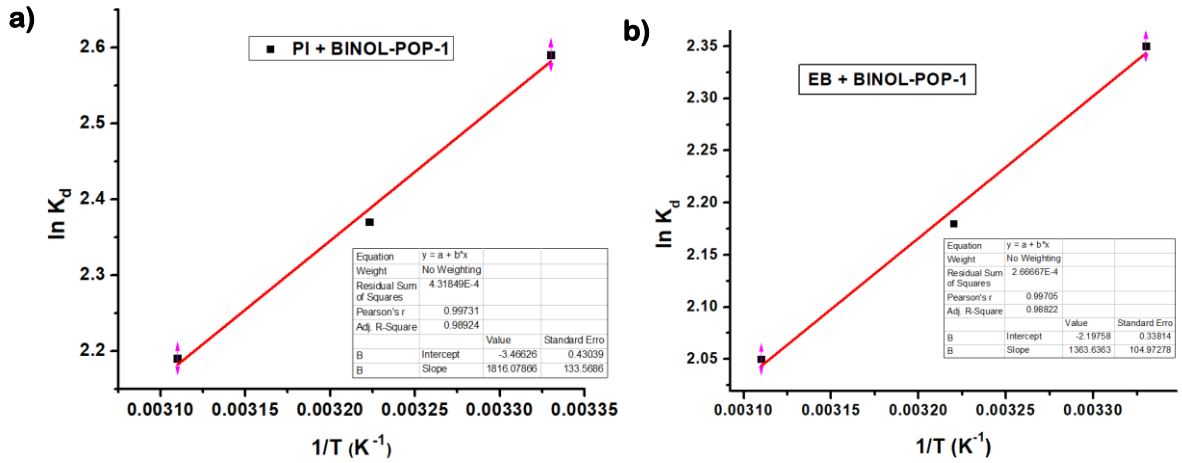

Fig. S23 lnK_d vs. 1/T plot for a) propidium iodide and b) ethidium bromide with **BINOL-POP-1.**

Table S11. Adsorption thermodynamic data for propidium iodide and **BINOL-POP-1.**

Temperature (K)	**lnK_d**	**ΔG (kJ/mol)**	**ΔS (kJ.mol^{-1}. K^{-1})**	**ΔH (kJ.mol^{-1})**
300	2.59	-6.46	-0.028	-15.098
310	2.37	-6.11		
320	2.19	-5.83		

Table S12. Adsorption thermodynamics for ethidium bromide with **BINOL-POP-1.**

Temperature (K)	**lnK_d**	**ΔG (kJ/mol)**	**ΔS (kJ.mol^{-1}. K^{-1})**	**ΔH (kJ.mol^{-1})**
300	2.35	-2.13	-0.018	-11.331
310	2.24	-2.07		
320	2.05	-1.91		

3.10 CAPTURING TEXTILE DYES:

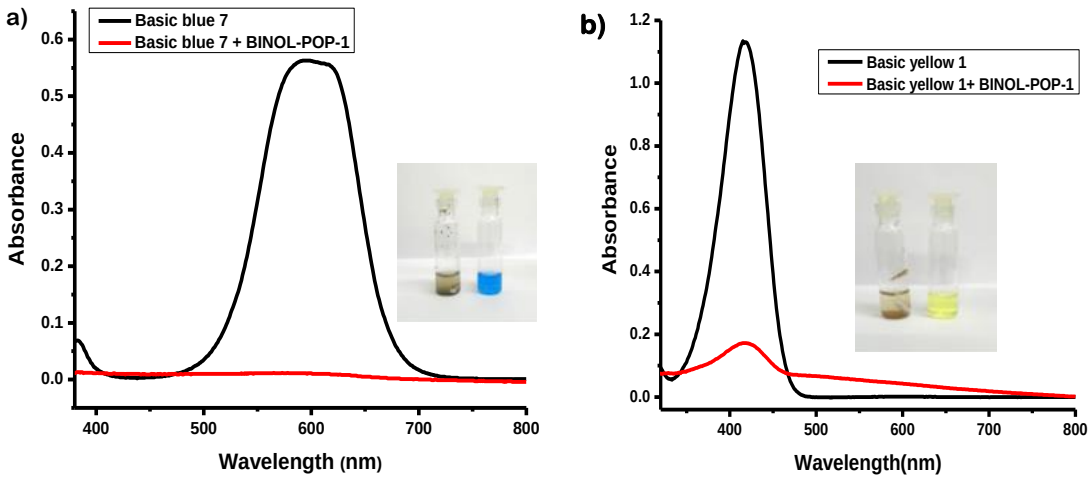

Fig. S24 a) Basic Blue 7 and b) Basic Yellow 1 adsorption using **BINOL-POP-1**. Inset images showing the corresponding aqueous solutions of the dye (right vial) and with **BINOL-POP-1** (left vial).

3.11 Adsorption isotherm fitting for BPA:

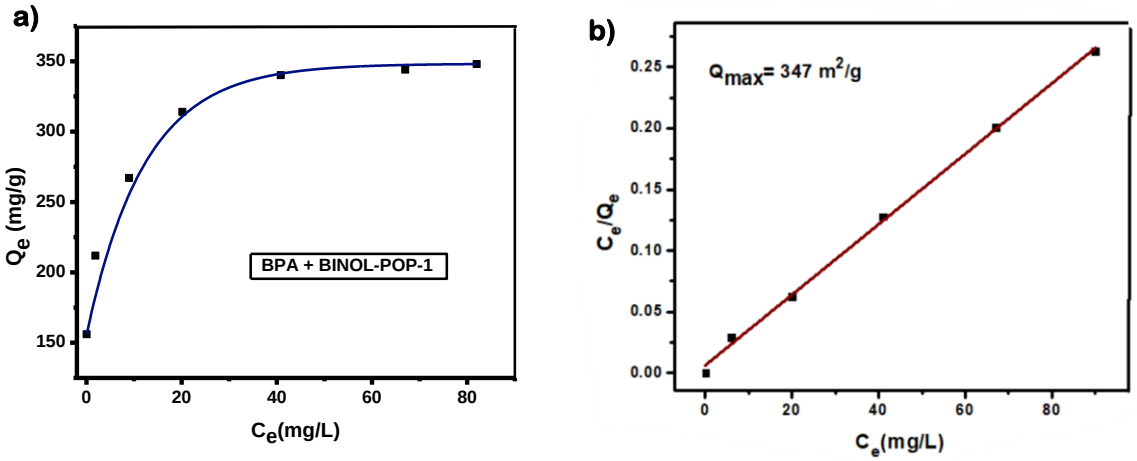

Fig. S25 a) Equilibrium adsorption capacity (Q_e) vs. equilibrium concentration of BPA(C_e) plot in water. b) Langmuir linear fit for BPA adsorption over **BINOL-POP-1**.

Computational findings for BPA adsorption:

The model was generated employing dispersion corrected DFT method. Hydrogen bond energy = 6.44 kcal/mol. After optimization, hydrogen bond length = 0.283 nm and π-π stacking energy = 3.21 kcal/mol

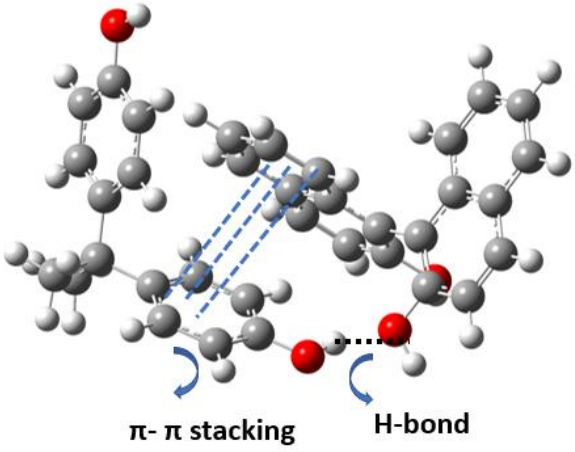

Fig. S26 DFT optimized interaction study for BPA and **BINOL** unit.

Reference:

1. M. S. Newman, V. Sankaran and D. R. Olson, Phenolic and ketonic tautomers in polycyclic aromatic hydrocarbons, *J. Am. Chem. Soc.*, 1976, **98**, 3237-3242.

2. S. Kanti Das, S. Mishra, K. Manna, U. Kayal, S. Mahapatra, K. Das Saha, S. Dalapati, G. P. Das, A. A. Mostafa and A. Bhaumik, A new triazine based π-conjugated mesoporous 2D covalent organic framework: its in vitro anticancer activities, *Chem. Commun.*, 2018, **54**, 11475-11478.

3. Y. Zhang, X. Hong, X.-M. Cao, X.-Q. Huang, B. Hu, S.-Y. Ding and H. Lin, Functional Porous Organic Polymers with Conjugated Triaryl Triazine as the Core for Superfast Adsorption Removal of Organic Dyes, *ACS Appl. Mater. Interfaces*, 2021, **13**, 6359-6366.
4. S. Dutta, S. K. Samanta and S. Bhattacharya, Phosphate based new organic polymer networks for efficient dye sorption and catalyst loading for chemo-selective reactivity, *Chem. Commun.*, 2022, **58**, 9405-9408.

5. M. Y. Lee, I. Ahmed, K. Yu, C.-S. Lee, K.-K. Kang, M.-S. Jang and W.-S. Ahn, Aqueous adsorption of bisphenol A over a porphyrinic porous organic polymer, *Chemosphere*, 2021, **265**, 129161.

6. M. Ge and H. Liu, A silsesquioxane-based thiophene-bridged hybrid nanoporous network as a highly efficient adsorbent for wastewater treatment, *J. Mater. Chem. A*, 2016, **4**, 16714-16722.

7. X. Yang and H. Liu, Ferrocene-Functionalized Silsesquioxane-Based Porous Polymer for Efficient Removal of Dyes and Heavy Metal Ions, *Chem. Eur. J*, 2018, **24**, 13504-13511.

8. X. Yang and H. Liu, Diphenylphosphine-Substituted Ferrocene/Silsesquioxane-Based Hybrid Porous Polymers as Highly Efficient Adsorbents for Water Treatment, *ACS Appl. Mater. Interfaces*, 2019, **11**, 26474-26482.

9. Y.-d. Chen, Y.-C. Lin, S.-H. Ho, Y. Zhou and N.-q. Ren, Highly efficient adsorption of dyes by biochar derived from pigments-extracted macroalgae pyrolyzed at different temperature, *Bioresour. Technol.*, 2018, **259**, 104-110.

10. X. Zhao, D. Wang, C. Xiang, F. Zhang, L. Liu, X. Zhou and H. Zhang, Facile Synthesis of Boron Organic Polymers for Efficient Removal and Separation of Methylene Blue, Rhodamine B, and Rhodamine 6G, *ACS Sustain. Chem. Eng.*, 2018, **6**, 16777-16787.

11. Y. Yuan, H. Huang, L. Chen and Y. Chen, N,N′-Bicarbazole: A Versatile Building Block toward the Construction of Conjugated Porous Polymers for CO_2 Capture and Dyes Adsorption, *Macromolecules*, 2017, **50**, 4993-5003.

12. L. Huang, M. He, B. Chen, Q. Cheng and B. Hu, Facile Green Synthesis of Magnetic Porous Organic Polymers for Rapid Removal and Separation of Methylene Blue, *ACS Sustain. Chem. Eng.*, 2017, **5**, 4050-4055.

13. Y. Du, M. Unno and H. Liu, Hybrid Nanoporous Materials Derived from Ladder- and Cage-Type Silsesquioxanes for Water Treatment, *ACS Appl. Nano Mater.*, 2020, **3**, 1535-1541.
14. B. Valley, B. Jing, M. Ferreira and Y. Zhu, Rapid and Efficient Coacervate Extraction of Cationic Industrial Dyes from Wastewater, *ACS Appl. Mater. Interfaces*, 2019, **11**, 7472-7478.

15. K.-Y. Yan, J.-Y. Chen, X.-Y. Li, Q. Wang and G.-C. Kuang, Carboxylic Acid Enriched Porous Organic Polymer as a Platform for Highly Efficient Removal of Methylene Blue from Aqueous Solution, *Macromol. Chem. Phys.*, 2020, **221**, 1900553.

16. N. Gibson, T.-J. M. Luo, O. Shenderova, Y.-J. Choi and D. W. Brenner, Modified Nanodiamonds for Adsorption of Propidium Iodide and Aflatoxin, *MRS Proc.*, 2009, **1236**, 1236-SS1209-1205.

17. N. M. Gibson, T. J. M. Luo, O. Shenderova, Y. J. Choi, Z. Fitzgerald and D. W. Brenner, Fluorescent dye adsorption on nanocarbon substrates through electrostatic interactions, *Diam. Relat. Mater.*, 2010, **19**, 234-237.

18. M. Iram, C. Guo, Y. Guan, A. Ishfaq and H. Liu, Adsorption and magnetic removal of neutral red dye from aqueous solution using Fe3O4 hollow nanospheres, *J. Hazard. Mater.*, 2010, **181**, 1039-1050.

19. F. M. Mpatani, A. A. Aryee, A. N. Kani, Q. Guo, E. Dovi, L. Qu, Z. Li and R. Han, Uptake of micropollutant-bisphenol A, methylene blue and neutral red onto a novel bagasse-β-cyclodextrin polymer by adsorption process, *Chemosphere*, 2020, **259**, 127439.

20. B. Heibati, K. Yetilmezsoy, M. A. Zazouli, S. Rodriguez-Couto, I. Tyagi, S. Agarwal and V. K. Gupta, Adsorption of ethidium bromide (EtBr) from aqueous solutions by natural pumice and aluminium-coated pumice, *J. Mol. Liq.*, 2016, **213**, 41-47.

21. R. Sulthana, S. N. Taqui, F. Zameer, U. T. Syed and A. A. Syed, Adsorption of ethidium bromide from aqueous solution onto nutraceutical industrial fennel seed spent: Kinetics and thermodynamics modeling studies, *Int. J. Phytoremediation*, 2018, **20**, 1075-1086.

22. A. D. Becke, Density-functional thermochemistry. I. The effect of the exchange-only gradient correction, *J. Chem. Phys.*, 1992, **96**, 2155-2160.

23. C. Lee, W. Yang and R. G. Parr, Development of the Colle-Salvetti correlation-energy formula into a functional of the electron density, *Phys. Rev. B*, 1988, **37**, 785-789.

24. Gaussian 16, Revision B.01, M. J. Frisch, G. W. Trucks, H. B. Schlegel, G. E. Scuseria, M. A. Robb, J. R. Cheeseman, G. Scalmani, V. Barone, B. Mennucci, G. A. Petersson, H. Nakatsuji, M. Caricato, X. Li, H. P. Hratchian, A. F. Izmaylov, J. Bloino, G. Zheng, J. L. Sonnenberg, M. Hada, M. Ehara, K. Toyota, R. Fukuda, J. Hasegawa, M. Ishida, T. Nakajima, Y. Honda, O. Kitao, H. Nakai, T. Vreven, J. A. Montgomery, Jr., J. E. Peralta, F. Ogliaro, M. Bearpark, J. J. Heyd, E. Brothers, K. N. Kudin, V. N. Staroverov, R. Kobayashi, J. Normand, K. Raghavachari, A. Rendell, J. C. Burant, S. S. Iyengar, J. Tomasi, M. Cossi, N. Rega, J. M. Millam, M. Klene, J. E. Knox, J. B. Cross, V. Bakken, C. Adamo, J. Jaramillo, R. Gomperts, R. E. Stratmann, O. Yazyev, A. J. Austin, R. Cammi, C. Pomelli, J. W. Ochterski, R. L. Martin, K. Morokuma, V. G. Zakrzewski, G. A. Voth, P. Salvador, J. J. Dannenberg, S. Dapprich, A. D. Daniels, Ö. Farkas, J. B. Foresman, J. V. Ortiz, J. Cioslowski, and D. J. Fox, Gaussian, Inc., Wallingford CT, 2016.

25. R. Dennington, T. Keith and J. Millam, Gauss View Version 6.1.16, *Semichem Inc., Shawnee Mission*, 2009.

26. S. Grimme, J. Antony, S. Ehrlich and H. Krieg, A consistent and accurate ab initio parametrization of density functional dispersion correction (DFT-D) for the 94 elements H-Pu, *J. Chem. Phys.*, 2010, **132**, 154104.

27. S. Grimme, S. Ehrlich and L. Goerigk, Effect of the damping function in dispersion corrected density functional theory, *J. Comput. Chem.*, 2011, **32**, 1456–1465.

28. K. Szalewicz, S. J. Cole, W. Kol/os and R. J. Bartlett, A theoretical study of the water dimer interaction, *J. Chem. Phys.*, 1988, **89**, 3662–3673.

29. B. Saha and P. Kr. Bhattacharyya, Adsorption of amino acids on boron and/or nitrogen doped functionalized graphene: A Density Functional Study, *Comput Theor Chem*, 2016, **1086**, 45–51.

30. S. F. Boys and F. Bernardi, The calculation of small molecular interactions by the differences of separate total energies. Some procedures with reduced errors, *Mol. Phys.*, 1970, **19**, 553–566.